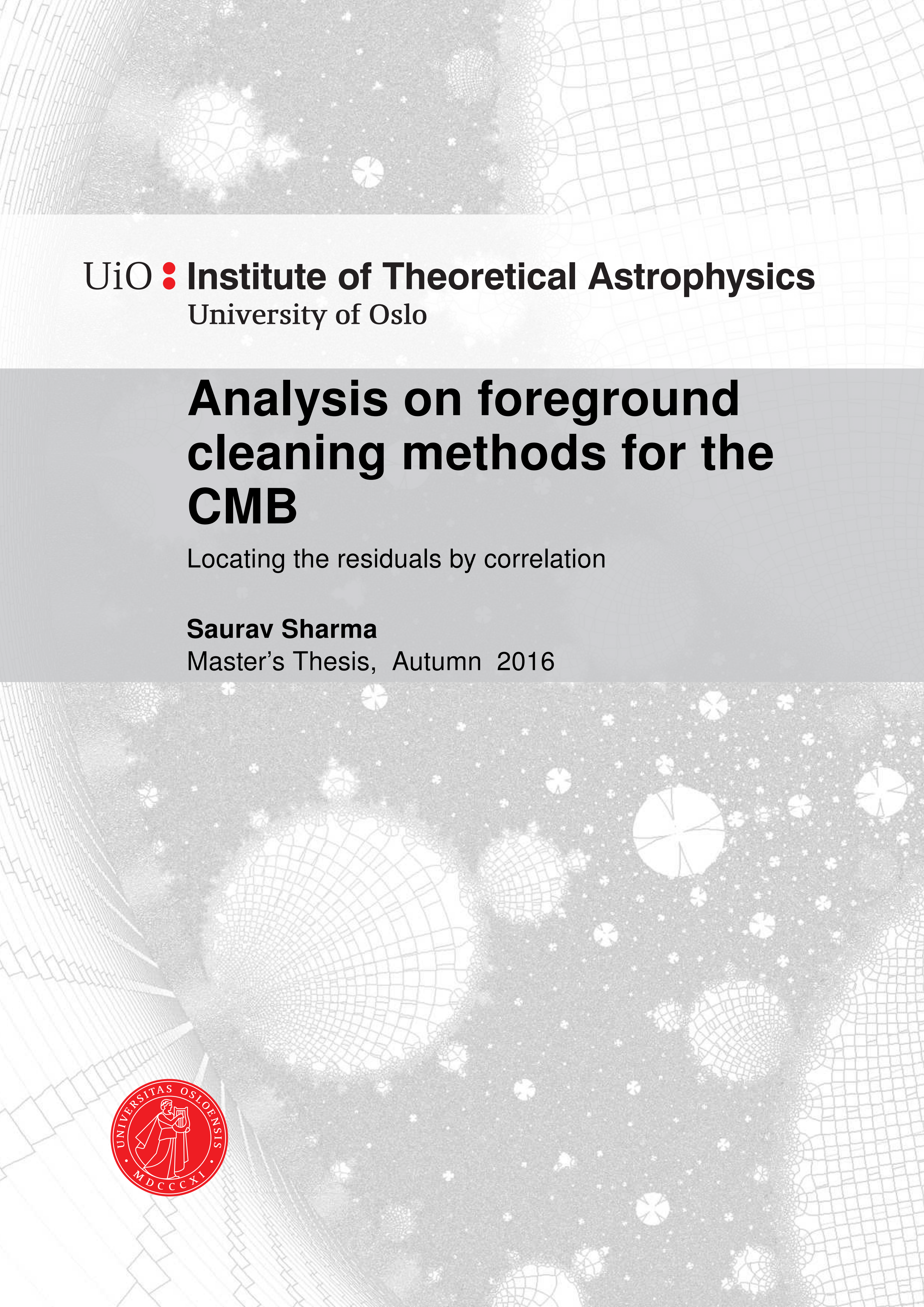

UiO : Institute of Theoretical Astrophysics
University of Oslo

Analysis on foreground cleaning methods for the CMB

Locating the residuals by correlation

Saurav Sharma
Master's Thesis, Autumn 2016

Abstract

In this thesis we are looking at the foreground cleaned maps of Smica, Sevem, NILC, and CR and trying to see if there are any residuals left after the cleaning. This is done by looking at the simulations for these methods and comparing them to the real Planck data. The simulations are used to make mean and standard deviation maps for each method, and also for combined maps where we take the difference of two of the maps so that we ideally only have the noise and foregrounds left. After that this is displayed on the form $\frac{x-\langle x\rangle}{\sigma_x}$. When we look it on this form we can see that there are some discrepancies near the galaxy, and we can explore this closer by looking at correlation coefficient between the difference maps and its components to find which method(s) contains the residuals. Looking at the correlation coefficient we see that the NILC and Smica methods have residuals of the same size, and that the Sevem method contains slightly less foreground than the previously mentioned methods but the difference is to small to be significant. The combinations with CR are to spread out to be certain, but for $j = 2$ CR has the least amount of residuals. The residuals are in general to big to say anything specific.

Acknowledgement

" Deadlines, a procrastinators best friend, and worst enemy."
I would like to thank my supervisor Frode Kristian Hansen for all the help i needed during my work with this thesis.

I would also like to thank especially Delmon Arous for all the help, and Aleksander Gravdahl Brzyski for the friendly rivalry, and of course all the professors and fellow students, you know who you are, as I hate to read, but love to ask.

Contents

Abstract iii

Acknowledgement v

1 Introduction 1

1.1 Motivation and the CMB . . . 2

2 Foregrounds and Cleaning Methods 3

2.1 Foregrounds . . . 4

2.1.1 Thermal Dust . . . 4

2.1.2 Free-Free . . . 5

2.1.3 Synchrotron . . . 5

2.2 Filtering methods . . . 5

2.2.1 SMICA . . . 6

2.2.2 SEVEM . . . 7

2.2.3 NILC . . . 7

2.2.4 CR . . . 7

3 Theory & Notation 9

3.1 Spherical Harmonics . . . 9

3.2 Power spectrum . . . 10

3.3 Wavelets & Needlets . . . 12

3.3.1 Wavelets . . . 12

3.3.2 Needlets . . . 14

3.4 Notation . . . 15

3.4.1 Bands and masks . . . 15

3.4.2 Scales . . . 16

3.5 Mean & Standard deviation . . . 17

3.6 Correlation coefficients . . . 17

4 Computations **19**
- 4.1 Short overview . . . 19
- 4.2 Single Method analysis . . . 19
- 4.3 Difference Map . . . 20
- 4.4 Cross Correlation . . . 21

5 Results and Discussion **25**
  - 5.0.1 Axelsson et al. 2014[1] . . . 25
  - 5.0.2 Goal of the thesis . . . 25
- 5.1 Replicated work . . . 25
- 5.2 Correlation coefficients . . . 26
- 5.3 Conclusion . . . 26
- 5.4 Sources of error . . . 27

6 Further Work **33**

List of Figures **35**

Bibliography **37**

Chapter 1

Introduction

In 1965, when Arno A. Penzias and Robert W. Wilson first found some irritating "noise" while testing their sensitive horn antenna, we have tried to remove contaminations from this "noise" that we today call cosmic microwave background, or CMB. From that point on we have looked at the CMB and tried to get a better view into the earlier stage of the universe. The CMB is the earliest light that was bouncing around in the cosmic plasma almost 14 billion years ago, and when the plasma got cold enough, so that the light and matter could decouple, the plasma became transparent to these photons, and they began to fly all over the universe and hit our antennas today. But there is a big problem that occurs when we try to take measurements of the CMB, and that is that not all the light that arrives to the antenna is CMB light, some of this light might be starlight, radiation from dust etc, which we are not interested in. Most of this contamination of the CMB comes from our own galaxy, and this is also going to be the focus in this thesis. What we have to do is to make a filter that excludes light from our galaxy, as well as hundreds of smaller points all over the sky which we know are stars contributing to the signal that is observed. This has already been done and the methods that we are going to look closer at in this thesis are SMICA, SEVEM, NILC, and CR. These methods use different approaches to remove these foreground, and what we are going to do in this thesis is to look at which of these methods leave the most residuals of the foreground in the signal. To do that we are looking at the results obtained from Axelsson et al. 2014 [1], and building on those results to find which of these methods are the most reliable.

1.1 Motivation and the CMB

So why are we interested in foreground cleaned CMB maps. To understand this we have to go back to the Big Bang. Right after the Big Bang we have a period called the inflationary period which lasted from about 10^{-36} to 10^{-33} seconds. In this time the whole universe expanded exponentially, but due to the small size of the universe at the start of this period, there were small fluctuation in this inflation field due to quantum effects.

So from about 10^{-33} seconds until about 380 000 years after the Big Bang, we have a hot soup, plasma, of particles and photons that we know from the standard model of particle physics interacting with each other. But as we know when something expands in a closed system it cools down, and when the temperature became cold enough, quarks bound together to form neutrons and protons, and eventually it became cold enough so that the protons no longer got ionized by the high energy photons, and the photons and matter decoupled.

Today we can then observe these photons to find out how the distribution was in the early stage of the universe. And by looking at this distribution we can try to find out how this inflationary field looks like, and try to understand what happened just a fraction of a fraction after the Big Bang.

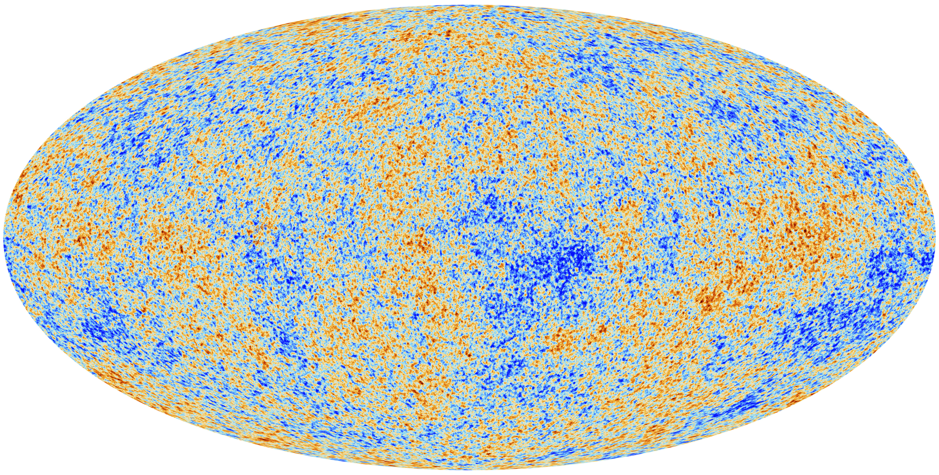

Figure 1.1: Here we can see a map of the CMB fluctuation. The temperature of the CMB is about 2.7 degrees Kelvin with fluctuations being on the order of 10^{-5} degrees.
Image source: http://sci.esa.int/science-e-media/img/61/Planck_CMB_Mollweide_4k.jpg

.

Chapter 2

Foregrounds and Cleaning Methods

In this part of the thesis we will go through some of the different foregrounds that occurs and also look quickly at how the methods try to separate the foreground from the actual CMB.

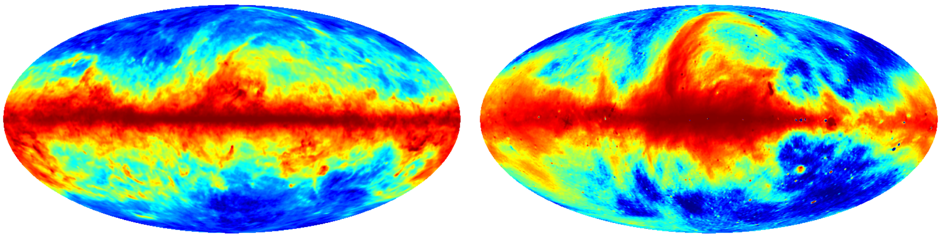

Figure 2.1: In these maps we can see examples of dust foreground on the left and synchrotron foreground on the right. Using maps like these one can try to subtract this from the signal. The subtraction is done differently for all the methods. In addition to dust and synchrotron, we have more foregrounds like, spinning dust, Free-free, CO molecular clouds, and more. Everything that is in between the CMB and our measuring devices is in fact foregrounds.
Left image: `http://pla.esac.esa.int/ftp_public/anonymous444476/maps/PR2/postcards/COM_CompMap_dust-commander_0256_R2.00.png`
Right image: `http://pla.esac.esa.int/ftp_public/anonymous444478/maps/PR2/postcards/COM_CompMap_Synchrotron-commander_0256_R2.00.png`

.

2.1 Foregrounds

As has been stated earlier, we don't only measure the CMB but also light from other sources. These sources emit light at different frequencies so when we try to measure the CMB, we should try to do it at different frequencies as we will be able to see different parts of the foregrounds better at different frequencies, meaning that we can locate them easier.

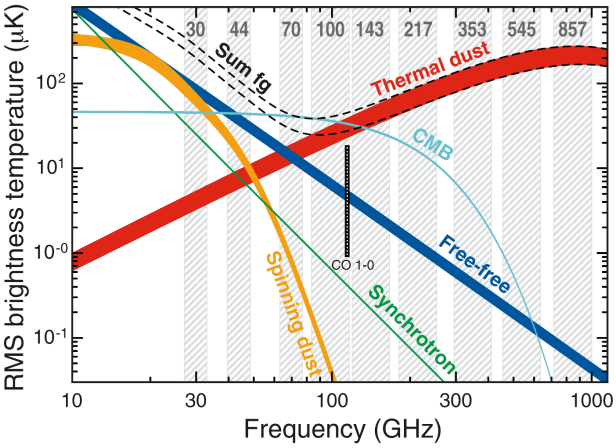

Figure 2.2: Illustration of the foreground contamination at different frequencies. On the x-axis one can see the frequencies and on the y-axis the brightness temperature. One can also observe some gray columns in this plot, and they are the different frequency bands that the Planck satellite observes at. Image source: http://lambda.gsfc.nasa.gov/product/foreground/

.

The foreground consist of everything that is between us and the CMB, but to name everything that might have an effect on the CMB would more or less impossible, so we will include some of the more important foregrounds. In figure 2.2 one can also see the distribution one expects from the different foregrounds.

2.1.1 Thermal Dust

The photons that are added to the signal as foreground that comes from thermal dust, are the photons associated with black body radiation. This means that the photons are emitted as heat from the dust. So the frequency that is emitted are dependent on the temperature of the dust clouds. The spacial region where we can find these clouds of dust are mostly near formed galaxies, where star formation is taking place, or the remnants from the death of a star.

2.1.2 Free-Free

Free-Free radiation or bremsstrahlung, is emission or scattering of photons that interact with charged particles, electrons or ions. This means that the source of these photons are from clouds of ionized gas, which mainly is localized in areas with high energetic photons that can ionize the gas.

2.1.3 Synchrotron

Synchrotron radiation is created when relativistic charged particles are accelerated, spiral through magnetic fields. This means that the radiation need two things, high velocity particles (electrons), and magnetic fields. Both of these can be found near pulsars or black holes.

2.2 Filtering Methods, Planck XII 2013[2], Ichiki 2014[3]

In this thesis we have focused on the comparison of 4 methods, SMICA, SEVEM, NILC, and CR. These are some different methods of removing foreground and noise from the signal. These methods are first looked at separately in the Single method analysis, and then combined two of them together to create difference maps that we do some statistical analysis on.

Situation			
Single Method		Combined	
index	Method	index	Difference
0	SMICA	0	SEVEM-NILC
1	SEVEM	1	NILC-SMICA
2	NILC	2	SMICA-SEVEM
3	CR	3	CR-SMICA
		4	SEVEM-CR
		5	NILC-CR

The Planck satellite observes the CMB on 9 different frequencies (the frequencies can be seen in figure 2.2). These observations from the satellite are then used in different ways to try to remove foregrounds.

2.2.1 (SMICA) Spectral Matching Independent Component Analysis

The principle of SMICA is to use data from all of the frequencies from the Planck satellite, and combine them with weights that vary over the multipole l, in spherical harmonic space (More on spherical harmonics in section 3.1).

So what one first do is to take the data from different frequencies and try to remove or fill in point sources on the maps. After this the data are transformed into spherical harmonic functions with $l_{max} = 4000$. The maps for the different frequencies are then combined with weights as shown in figure 2.3. To simplify independent spectral analysis one takes

$$x^j = A_i^j s^i \tag{2.1}$$

Where x^j is the observed intensity at frequency j, s^i is the signal including foregrounds, and A_i^j is the mixing matrix. All of this is done in spherical harmonic space. (See section 3.1 for more info)

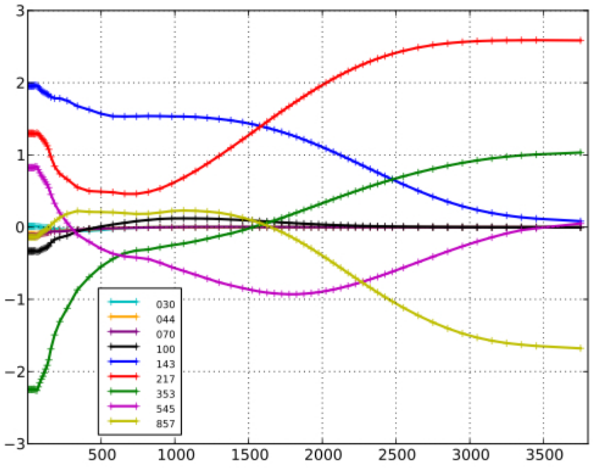

Figure 2.3: Here we can see the weighting for the different frequencies over the multipoles up to $l_{max} = 4000$
Image source: `https://wiki.cosmos.esa.int/planckpla/images/9/93/Smica.jpg`

.

2.2.2 (SEVEM) Spectral Estimation Via Expectation Maximation

The principal behind Sevem is to take data from two different frequencies to make templates. These templates should then only contain foregrounds from one or more of the foregrounds named earlier and then used to remove the foregrounds from the data from a third frequency.

Sevem only assumes one thing and that is that the CMB, $T(pix,\nu)$, is given as a combination of various components, $X_i(pix)$, and noise, $n(pix,\nu)$. This means that the signal can be written as

$$T(pix,\nu) = \sum_i \alpha_i(\nu) X_i(pix) + n(pix,\nu) \tag{2.2}$$

where α are the template coefficients. By looking at the signal in such a way we can try to eliminate foregrounds from the maps that are not used in making the templates.

2.2.3 (NILC) Needlet Internal Linear Combination

The principle behind the NILC method is to know how the CMB should behave. Using this knowledge we make a model of the observed signal and try to minimize the variance so that we only have the CMB signal left in our maps.

As the methods says we are doing this in Needlet-space (More on needlets in section 3.3). What we do is to assume that the observed signal is on the form

$$x^j_{lm} = a^j s_{lm} + f^j_{lm} + n^j_{lm} \tag{2.3}$$

Here s_{lm} is the signal that we want to have, f_{lm} and n_{lm} are the foreground and noise respectively. j here denotes the frequency that is looked at, and l and m are the multipole notation. By representing the signal in this way we can then weight components $\hat{s}_{lm} = \boldsymbol{w}_l^\dagger \boldsymbol{x}_{lm}$ to try to minimize the variance of $\hat{s}$, with the restrain that $\boldsymbol{w}_l^\dagger \cdot \boldsymbol{a} = 1$. This is done in needletspace (section 3.3) and does not include the 30GHz band in the Planck data.

2.2.4 (CR) Commander-Ruler

The principle behind the Commander-Ruler is to set up equations for the foreground and assume that the observed signal can be split up in 3 part, CMB, foregrounds and noise. Once we have the observed data one can try to fit the signal in each pixel by tweaking the parameters for the foreground.

The methods is iterative and assumes that the observed signal $\boldsymbol{d}$ can be split up into CMB signal, $\boldsymbol{s}$, and foreground $\boldsymbol{f}$. Meaning that you get

$$\{\boldsymbol{s}, \boldsymbol{f}\}^{(i+1)} \longleftarrow P(\boldsymbol{s}, \boldsymbol{f}|C_l^{(i)}, \boldsymbol{d}) \tag{2.4}$$

$$C_l^{(i+1)} \longleftarrow P(C_l|\boldsymbol{s}^{(i+1)}) \tag{2.5}$$

where we have that

$$P(\boldsymbol{s}, \boldsymbol{f}|C_l^{(i)}, \boldsymbol{d}) \propto \exp(-\frac{1}{2}\sum_{\nu}(\boldsymbol{d}_\nu - \boldsymbol{s}_\nu - \boldsymbol{f}_\nu)^T \boldsymbol{N}_\nu^{-1}(\boldsymbol{d}_\nu - \boldsymbol{s}_\nu - \boldsymbol{f}_\nu)) \exp(-\frac{1}{2}\boldsymbol{s}^T \boldsymbol{S}^{-1}\boldsymbol{s}) \tag{2.6}$$

$$P(C_l|\boldsymbol{s}^{(i+1)}) \propto \exp(-\frac{1}{2}\boldsymbol{s}^T \boldsymbol{S}^{-1}\boldsymbol{s}) \propto \exp(-\frac{1}{2}(2l+1)\frac{\sigma_l^2}{C_l}) \tag{2.7}$$

where $\boldsymbol{N}_\nu$ is the noise covariance at frequency ν, $\boldsymbol{S}$ is the signal covariance and σ_l^2 is the variance of the estimated signal. This is done for each pixel and only includes data from 30-353 GHz.

Chapter 3

Theory & Notation

In this part we will quickly go though the basics of the theory, notation, and formulation that is used in the rest of this thesis.

When we look at the sky we are looking at a scalar field, but there is no preferred direction to look at, so we need to make our own standard orientation. What we do is to say that the scalar field we are looking at looks like $T(\theta, \phi)$, where we use galactic co-latitude and longitude. This means that for $\theta = 0°$ we are looking at the galactic north pole, and $\theta = 180°$ is the galactic south pole, going through the galactic center for $\phi = 0°$, with $\phi = [0, 360°]$. There are many more way to represent this scalar field instead of just with spherical coordinates, and some of them are:

3.1 Spherical Harmonics

Spherical harmonics is to a sphere what Fourier series is to a signal in 1D. Both methods can be used to represent any signal in their respectively domains. For spherical harmonics we have that the signal can be determined by.

$$T(\theta, \phi) = \sum_{l=0}^{\infty} \sum_{m=-l}^{l} a_{lm} Y_{lm}^{*}(\theta, \phi) \tag{3.1}$$

Where a_{lm} are the spherical harmonic coefficients, and $Y_{lm}(\theta, \phi)$, are the spherical harmonic functions. We can then, similarly as for Fourier series, find the spherical harmonic coefficients by.

$$a_{lm} = \int d\theta d\phi \sin(\theta) T(\theta, \phi) Y_{lm}^{*}(\theta, \phi) = \int d(\cos\theta) d\phi T(\theta, \phi) Y_{lm}^{*}(\theta, \phi) \tag{3.2}$$

As we see from equation 3.1, we ideally want a l value that is infinitely large. But as we can't get l infinitely large, we choose a l_{max} large enough so that the resolution of our image is smaller and that this discrepancy can be looked at as small scale noise. As we are only interested in the fluctuations in the temperature, we usually remove the mono- and dipole from the signal. The monopole is removed so that the signal only contains fluctuations and not the background temperature. The dipole is removed because the Earth has a velocity in comparison to the rest frame of the CMB, and this motion will cause a shift in the observed data due to the Doppler effect.

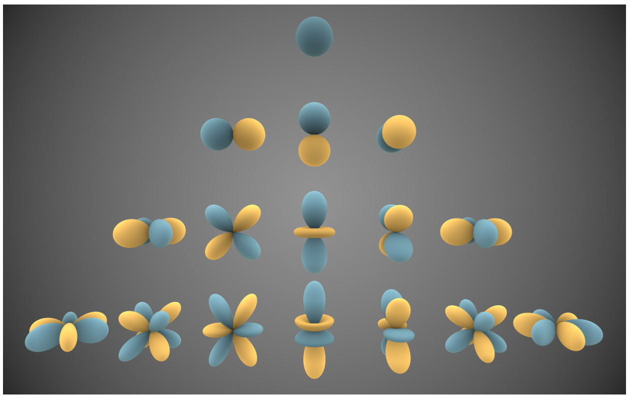

Figure 3.1: In this figure we can see the spherical harmonic functions for the first 4 multipoles with different values of m. The distance from the origin shows the amplitude of the function and the colors show if the value is positive (blue) or negative (yellow).
Image source: `https://upload.wikimedia.org/wikipedia/commons/6/62/Spherical_Harmonics.png`

.

The multipole l says something about how big of a structure we are looking at in the sky. For $l = 0$ we are looking at the average background temperature (monopole), being the largest scales, to smaller and smaller scales for increasing values of l. To get an idea for how big the angular resolution is for a given multipole we have that $\theta \propto \dfrac{180^\circ}{l}$.

3.2 Power spectrum

Now that we are only left with the fluctuations in the field, we can try to look at it in a simpler way. What we can do is to try to look at the variance of the harmonic coefficients which is on the form,

$$\langle a_{lm} a^*_{lm} \rangle = \delta_{ll'} \delta_{mm'} C_l \tag{3.3}$$

Where C_l is the angular power spectrum and contains the information of the fluctuations from the data. The power spectrum is a nice tool as we get all the information but now with only one variable to keep track on being the multipole l.

We can estimate the power spectrum by

$$C_l \approx \sum_{m=-l}^{l} \frac{a_{lm} a^*_{lm}}{2l+1} \tag{3.4}$$

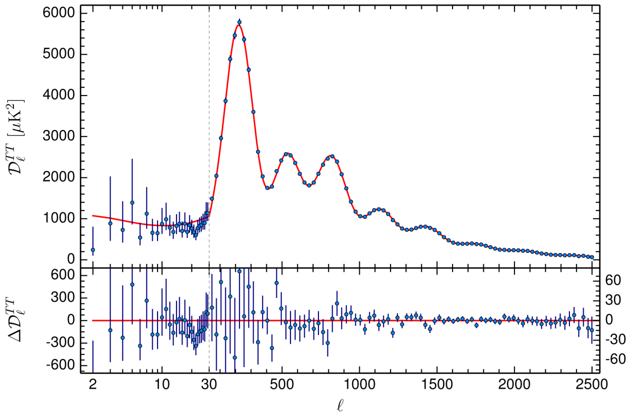

Figure 3.2: In this figure we can see an example of the power spectrum with fitted data
Image source: http://www.cosmos.esa.int/documents/387566/425793/2015_TTSpectrum/d03dcc5f-a9a4-42df-be5b-fd0bdc5d956a?t=1423087098010

.

As we now have an easier way to look at the information from the observed CMB, in the power spectrum, it becomes easier to show why it is so important to get a accurate as possible picture of the CMB. From the Power spectrum, we can get lots of information about how our universe is put together, and can aid us in checking what theories have the most substance to them.

So by location peaks and troughs in both multipole range and amplitude, and by looking at ratios between the peaks we can take get information on cosmological parameters, inflationary models, initial conditions in the universe etc. One example on how the power spectrum may change can be seen in figure 3.4.

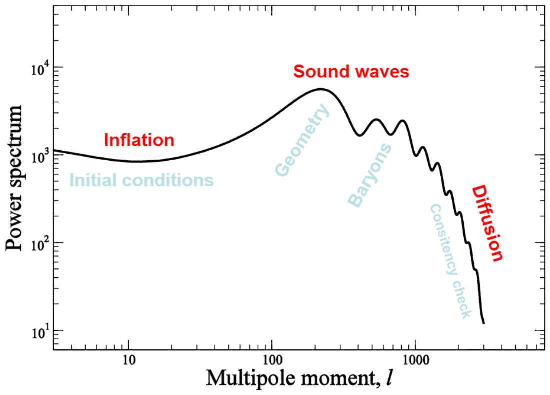

Figure 3.3: Each range of multipoles gives us some indication to the mixture of cosmological parameters and initial conditions in the universe.
Image source: Slides from a course with H.K.K. Eriksen

.

3.3 Wavelets & Needlets

3.3.1 Wavelets

When we are looking at a signal in 1D, it is nice to know that the signal have different frequency contributions in it, but with Fourier it is hard to know where in the signal these frequencies comes from. What is done then is to use a windowed Fourier, or short-time Fourier transform. This means that you slice up the signal you have into different pieces and take a Fourier transform on the smaller parts. This will give you a better time resolution, but can introduce some frequency bleeding, or frequency leaking. This means that a sharp frequency peak, can be diffused if the slicing is not done correctly, and also introduces other problems that is controlled better by wavelets.

Wavelets is basically the same as a windowed Fourier transform, the only major difference being that the wavelet transform is specially designed for locating in both time and frequency domain. Further the wavelet transform is done the same way as Fourier transform.

$$X(a,b) = \int_{-\infty}^{\infty} x(t)\psi^*_{a,b}(t)dt \tag{3.5}$$

where we now have that the output $X(a,b)$ is a matrix of scales and translation instead of a only frequency. i addition to that the function we use $\psi_{a,b}(t)$ is also different and has some constrains to it, the minimum being

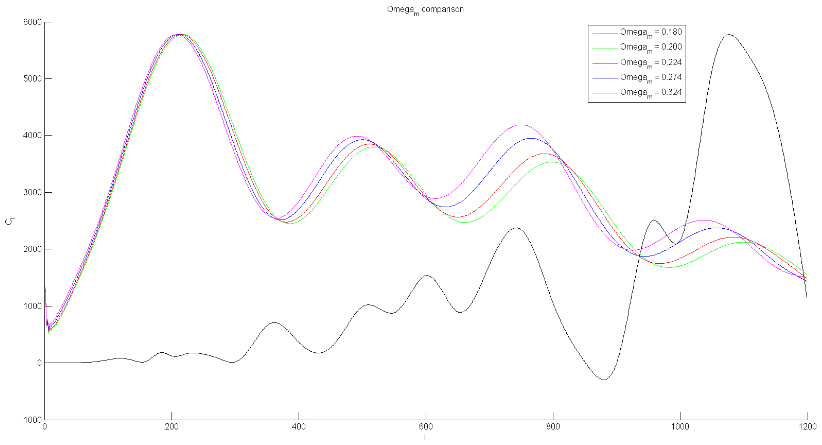

Figure 3.4: Changing the density of the dark matter affect the height and position of the third peak. The more dark matter that is present the bigger the gravitational potential is and therefore more and bigger structures are created. If there so little dark matter that they can not form strong enough potentials for the baryonic matter to fall in we get the black curve where we only have very small structures due to the photon pressure in the early universe.
Image source: From project in course with H.K.K. Eriksen

.

that

$$\int_{-\infty}^{\infty} \psi(t)dt = 0 \tag{3.6}$$

Further there are some other restrains to the wavelets. Because we both want time localization and frequency localization, we meet a boundary that is know to all physicists. There is a trade-off how fine the resolution can be in time and frequency due to the Heisenberg uncertainty principle. This means that we need to make sure we choose the right resolution.

So when we are looking at different sizes what usually is done is to scale the mother wavelet, basis wavelet, as follows

$$\psi_{m,n}(t) = 2^{-\frac{m}{2}} \psi(2^{-m}t - n) \tag{3.7}$$

With wavelets we can locate frequencies or structures in 1D and 2D, but for flat geometries. To do this on a sphere we have to move over to needlets.

3.3.2 Needlets (Marinucci et al. 2008)[4]

So when we are trying to locate the structures on the sphere we have to move over to needlets instead of wavelets. This is done because wavelets can't directly map over from a plane to the sphere. One might also ask why we bother with using needlets when we have spherical harmonics functions. The answer is simple, if we were using the whole dataset and not a subset of it, spherical harmonics would be perfect. We are using the standard U73 mask (figure 3.5 for more details), which only uses about 73% of the sky. this means that we need to know where the structure are located and that we don't get any ringing, or other artifacts in the statistical analysis we want to do later on.

So the needlets functions are defined as

$$\psi_{jk}(\hat{\gamma}) = \sqrt{\lambda_{jk}} \sum_{l} b(\frac{l}{B^j}) \sum_{m=-l}^{l} \bar{Y}_{lm}(\hat{\gamma}) Y_{lm}(\xi_{jk}) \tag{3.8}$$

where we have that λ_{jk} are the weights for the pixels in the map denoted by ξ_{jk} for scale j. Further we have $\sum_{m=-l}^{l} \bar{Y}_{lm}(\hat{\gamma}) Y_{lm}(\xi_{jk})$ can be looked at as a projection with a window function defined by $b(\frac{l}{B^j})$. There are of course some restrictions to this window function:

1. $b^2(\cdot)$ has support in $[\frac{1}{B}, B]$ giving that $b(\frac{l}{B^j})$ has support in $l \epsilon [B^{j-1}, B^{j+1}]$
2. the function is infinitely differentiable in $(0, \infty)$
3. $\sum_{j=1}^{\infty} b^2(\frac{l}{B^j}) \equiv 1$ for all $l \geq B$.

This can be achieved by making this window using the following steps.

$$f(t) = \begin{cases} \exp(-\frac{1}{1-t^2}), & -1 \leq t \leq 1 \\ 0, & \text{otherwise} \end{cases} \tag{3.9}$$

Then we take this function so that

$$\psi(u) = \frac{\int_{-1}^{u} f(t)dt}{\int_{-1}^{1} f(t)dt} \tag{3.10}$$

This is new function is taken further so that

$$\phi(t) = \begin{cases} 1, & 0 \leq t \leq \frac{1}{B} \\ \psi(1 - \frac{2B}{B-1}(t - \frac{1}{B})), & \frac{1}{B} \leq t \leq 1 \\ 0, & t \geq 1 \end{cases} \tag{3.11}$$

and finally we get that the needlet function is

$$b^2(\xi) = \phi(\frac{\xi}{B}) - \phi(\xi) \tag{3.12}$$

Where the positive function is chosen for $b(\xi) = [\phi(\frac{\xi}{B}) - \phi(\xi)]^{1/2}$

3.4 Notation

3.4.1 Bands and masks

When we do the statistical analysis on the CMB there are some part of the sky that are not used. What is needed to be done is to remove or mask out some parts of the sky. Initially we use the U73 mask that removes our galaxy and hundreds of other point sources from the data. What is done further is to split this U73-mask into bands. The two bands closest to the galaxy, right north of and south of the galaxy, are combined and called band 1. Going outwards we get band 2 and so on until we reach the poles which combine to give us band 7. This can be seen in Figure 3.5.

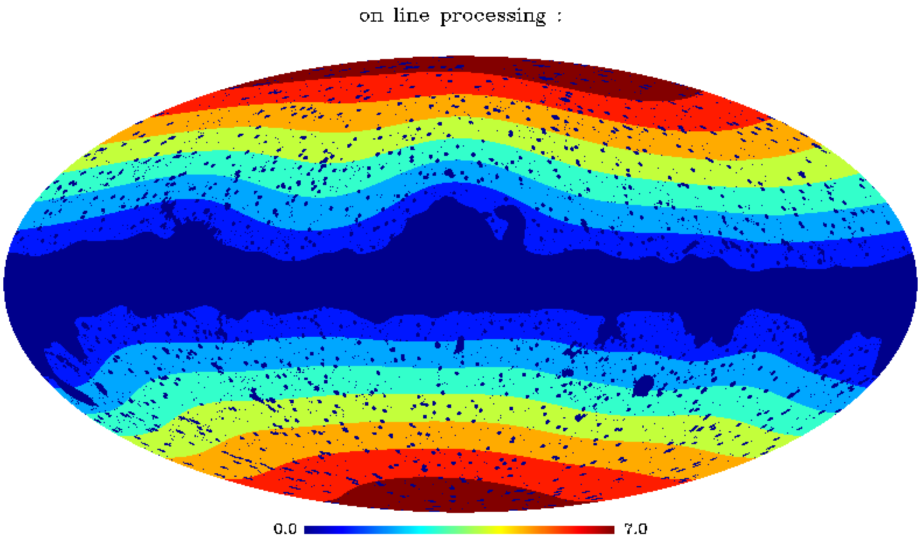

Figure 3.5: In this figure we can see how the bands are layed out in the U73 mask. The darkest of the blue colors is not included. So all the dark blue spots and center of the galaxy are masked out completely

.

3.4.2 Scales

In this thesis we look at the data in different bands and for different methods. But in addition to that we do one more split being that we are looking at different scales, or looking for different sizes on the sky. As mentioned earlier we have that just as in Fourier transform looking at small values of l means that we look at big parts of the sky and vice versa. We have that the angular opening goes something like $\theta \propto \frac{360^\circ}{2l} = \frac{180^\circ}{l}$ for the spherical harmonics. But we are using standard needlets to cover the multipoles $l = [2, 1500]$, and as each needlet covers a range of multipoles $l\epsilon[B^{j-1}, B^{j+1}]$ and we are using standard needlets we know that $B = 1.8393$, which gives us that $j = [2, 11]$. And these j values are what we use further when we am talking about the scales. An example of the sizes of the different j values can be seen in Figure 3.6 (Needlets are a way to locate where the structures are)

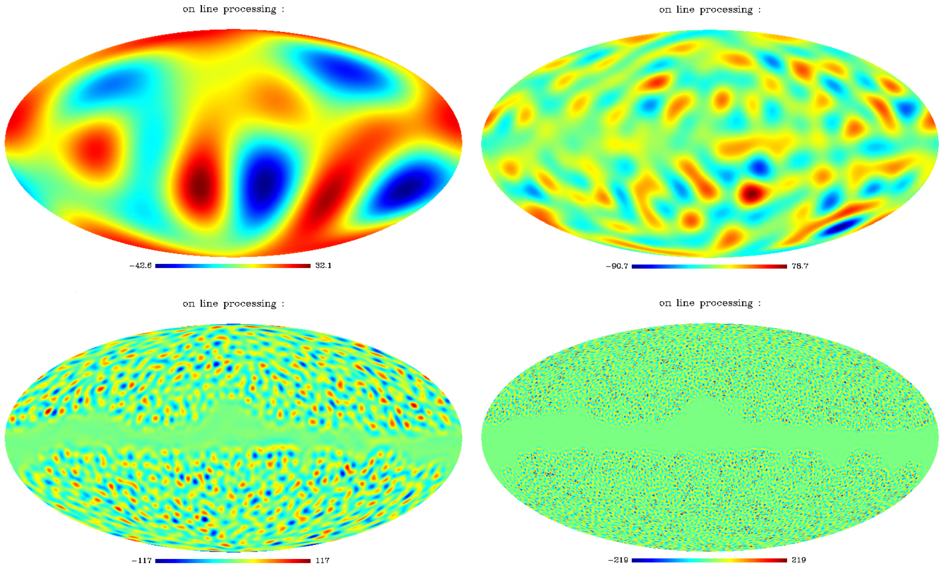

Figure 3.6: In this figure we can see we can see from the top left corner to the bottom right corner the needlet maps for one specific method with 4 of the values of j that are being used, being respectively 2,4,6, and 8. As we can see the lower values of j means that we look at more of the sky as one part and with higher values of j we really look at smaller part of the sky as a whole.

3.5 Mean & Standard deviation

In this part of the thesis we will **not** be going through the theory of how to compute the mean and standard deviation (sigma). This part is more like a warning that there will be many mean and sigmas throughout the rest of this thesis. As we are working with simulations of Planck maps there will be a mean for each pixel over simulations, meaning that we will add all the simulation together and find the mean for each pixel in the map. Similarly we will have a sigma for each pixel over the simulations.

Further as we are splitting the maps we have into methods, bands, and scales, we will compute the mean and sigma for these mean and sigma maps, meaning that we will take the mean of the mean values for each method, band, and scale. And also the mean for the sigma maps for each method, band, and scale. Not only that but we will also find the standard deviation for those mean and sigma maps in each method, band, and scale.

Later on these might be used to compute the correlation between single methods and the difference maps giving us some coefficients for each simulation. Further we need to find the mean and standard deviation for these coefficients as well.

All this is done so that we can display the results on the form

$$\frac{x - \langle x \rangle}{\sigma_x} \tag{3.13}$$

making it easier to look for discrepancies in the results.

3.6 Correlation coefficients

Correlation coefficients is a statistical representation of how two sets of data have a linear relationship to each other. One way of computing these coefficient is

$$\rho_{X,Y} = \frac{1}{N} \sum_{i=1}^{N} \frac{(X_i - \mu_X)(Y_i - \mu_Y)}{\sigma_X \sigma_Y} \tag{3.14}$$

, where $\rho_{X,Y}$ is the correlation coefficient between the data sets X and Y. N is the total number of data points in each set that we are taking the correlation over. X_i are the data points in the first data set with corresponding mean value (μ_X) and standard deviation (σ_X) for the given set. In the same way we have everything marked with Y for the other set of data points.

Chapter 4

Computations

4.1 Short overview

First we have taken the code that is used to get the result in Axelsson et al. 2014[1]. The code is split up in different sections and what we needed to do is to replicate the results from the sections for single method analysis and difference map analysis. Each of the sections are again split into a calibration part where we take 1000 simulations of the universe which are saved in .fits-files from each method and convert them to maps with different j-values, and then find the mean, standard deviation, and skew of each of the pixels. The calibration is also done separately for the difference maps before we introduce the actual Planck data. The work in the single method and difference maps can be done separately, but both are needed to do the final comparison of the methods. After this is checked to see that this works properly we can continue to build on it to compute the correlation coefficient.

The reproduction of the skewness from Axelsson et al. 2014[1] is also done for completeness but is not included in this thesis as it is something that is not used beyond checking that the code actually works.

4.2 Single Method analysis

First what is done is that we take the simulation data for each method, apply the U73 mask and convert them into needlet-maps. After this we need to find the mean and standard deviation over the simulations for each pixel in the map, and saved to files to conclude the calibration phase. Then we calculate the mean and standard deviation for the Planck data for each method, band,

and scale by

$$m_{ch,b,j} = \sum_{i=pixels} \frac{\beta_{i,ch,j}}{\sigma^2_{i,ch,j}} \times M_{i,b} \tag{4.1}$$

$$s_{ch,b,j} = \sum_{i=pixels} \frac{\beta^2_{i,ch,j}}{\sigma^4_{i,ch,j}} \times M_{i,b} \tag{4.2}$$

Where β is the Planck signal, σ is the standard deviation that we just got from the calibration M is the bandmask as we are doing this for each of the band. We are calculating the mean, $m_{ch,b,j}$, and the standard deviation, $s_{ch,b,j}$. All of this are done separately for each of the methods, bands and scales. (The subscript for method in ch)

After we have done this for the Planck data we use the simulations to find similar mean and standard deviation for each simulation. After that we can find the mean and standard deviation for all of these means and standard deviations. In other terms we have to find: (subscripts are dropped for method, band and scale)

$$\begin{aligned} \mu_m &= \frac{1}{N} \sum_{simulation} (\sum_{pixels} \frac{\beta_{sim}}{\sigma^2} \times M) \\ \mu_m &= \frac{1}{N} \sum_{simulation} (m_{ch,b,j})_{sim} \end{aligned} \tag{4.3}$$

and

$$\begin{aligned} \mu_s &= \frac{1}{N} \sum_{simulation} (\sum_{pixels} \frac{\beta^2_{sim}}{\sigma^4} \times M) \\ \mu_s &= \frac{1}{N} \sum_{simulation} (s_{ch,b,j})_{sim} \end{aligned} \tag{4.4}$$

and similarly we have to find the standard deviation of the mean and standard deviation σ_m and σ_s. This is done to obtain the plots on the form $\frac{x - <x>}{\sigma_x}$ where the variable x are computed from the Planck data and the mean and sigma for are computed from the simulations.(Results can be seen in figure 4.1)

4.3 Difference Map

The analysis for the difference map is almost the same as for the single method analysis. The only differences are that we are combining two of the methods to see if there are any discrepancies between them, and because we have to combine maps we have to smooth the maps so that we do the analysis with the resolution of the smallest map. The other thing that differs from the single method analysis is that in the comparison between the Planck data and simulation we before used $\frac{x-<x>}{\sigma_x}$. What we do now is to exchange σ_x to σ_{CMB} to see how large the residual is in comparison to the actual CMB signal. Besides from that we follow the same procedure as for the single method analysis.

4.4 Cross Correlation

After we have checked that the code for the single method analysis and difference map works we can start to implement the code for the correlation coefficients. As we are only interested in the coefficient for band 1, as that is where we have the largest discrepancy, we have to find the mean and standard deviation of the values in this band for each simulation. When this is done we can compute the coefficients for all of the simulations between the difference map, and each of its components, from the single method.

Now that we have all of the correlation coefficient we again want to display it on the form $\frac{x-\langle x\rangle}{\sigma_x}$, meaning that we need to find the mean and standard deviation of the coefficients. We then find the correlation coefficients from the Planck data and when this is done for all of the difference maps we are done with the code and can continue on to the results.

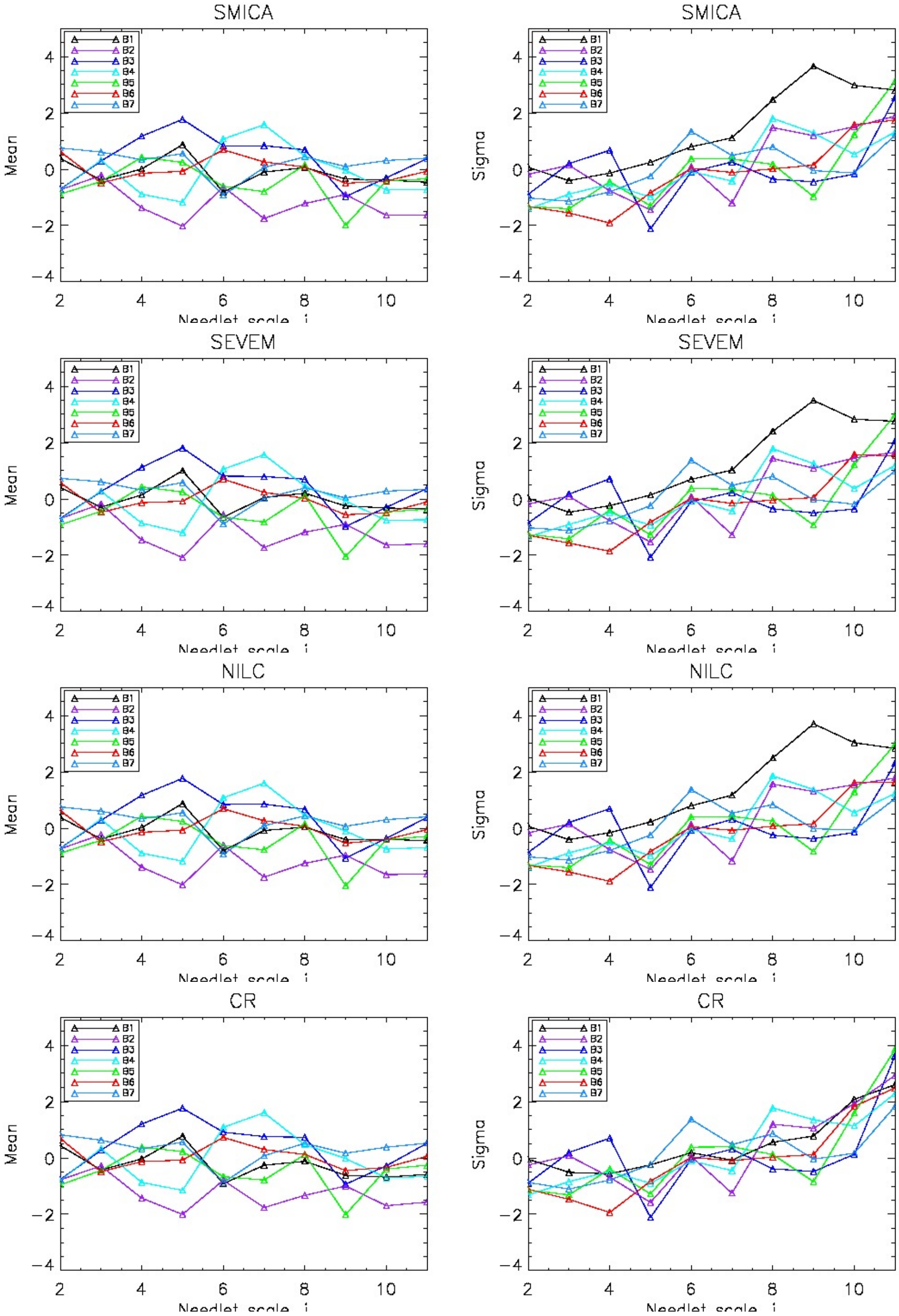

Figure 4.1: In this figure we have plotted on the form $\frac{x - \langle x \rangle}{\sigma_x}$. Where we have that x is either the mean(first column) or standard deviation(second column) for the different methods SMICA, SEVEM, NILC, and CR (each row). This is done to see if we can recreate the results from Axelsson et al. 2014[1] seen in figure 5.1

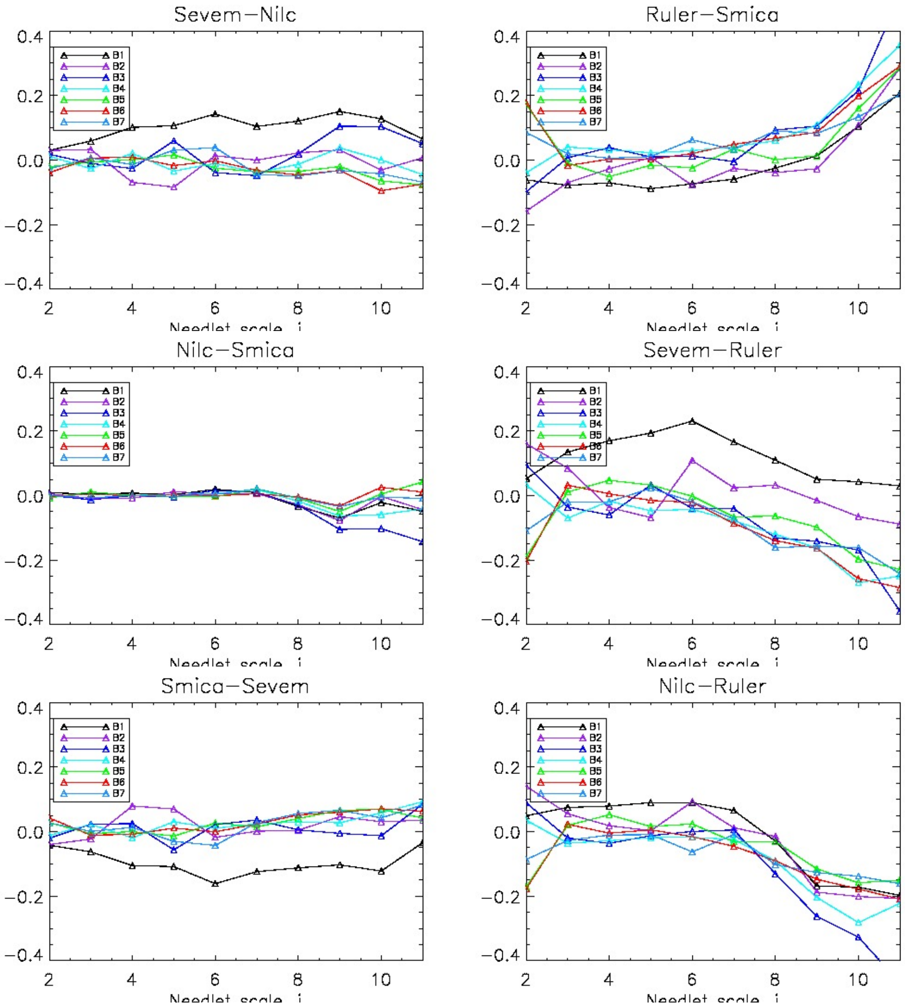

Figure 4.2: In these plots we are displaying the mean for the difference maps. Here we are again displaying the plots on the form $\frac{x - \langle x \rangle}{\sigma_{CMB}}$. Notice the difference from Single method analysis. Here we are dividing with the standard deviation of the CMB instead of the difference map to see how big of an influence residuals in the map may have on the CMB signal. This is being compared to figure 5.2 which we have gotten from Axelsson et al. 2014[1]. In the article they have only chosen a subset of the combinations so we are comparing these with only the left column in that figure.

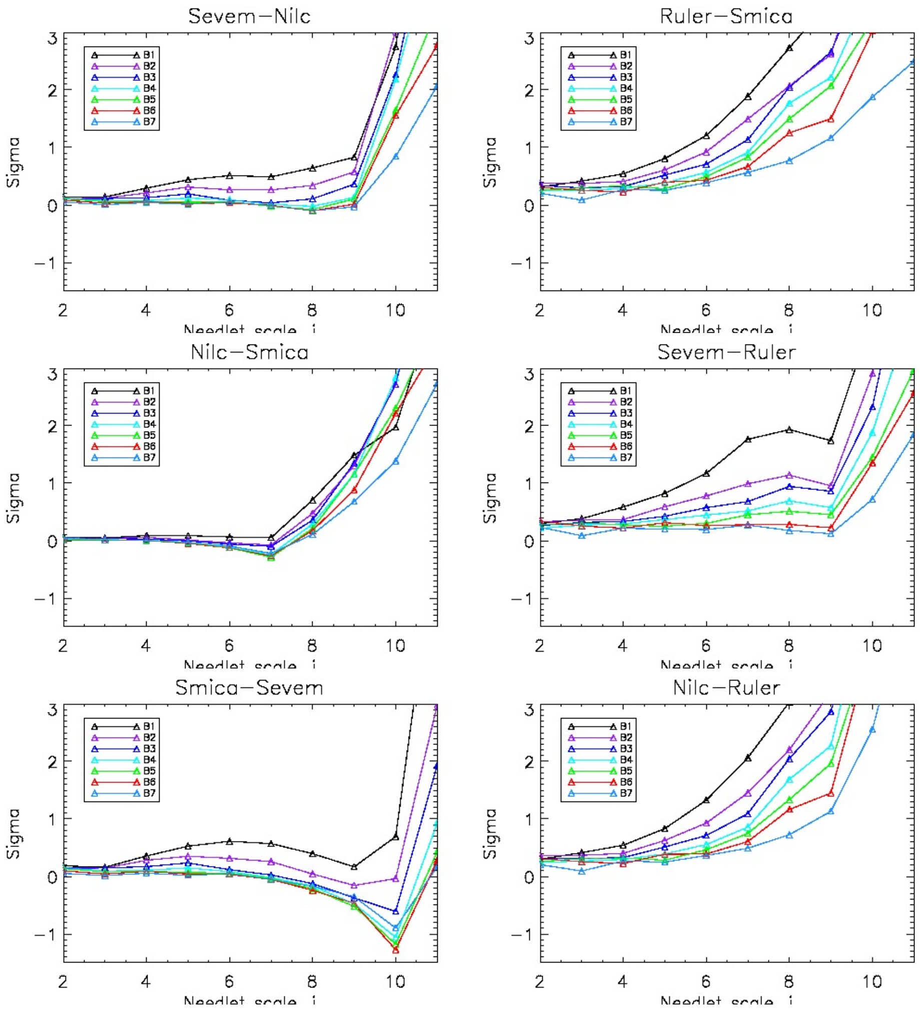

Figure 4.3: Just as in figure 4.2 but now we are displaying the standard deviation instead. Compared with the right column in figure 5.2 which is results from Axelsson et al. 2014[1]

Chapter 5

Results and Discussion

5.0.1 Axelsson et al. 2014[1]

In the article the analysis on single method and difference maps are done to find out if the U73 mask can be used reliably outside of the scope that it is used for now, and they are trying to find a new way of designing a confidence mask. They found out that the CR method had to much residuals in the difference maps and concluded that they due the rest of the analysis should exclude the CR method. In addition to that they also found the the complex foreground limited the analysis to $l_{max} \leq 1500$. Working with the remaining three methods it was concluded that the U73 mask should be extended so that more point sources were removed and a larger area around the galaxy was excluded, and concluded with a new confidence mask named U66.

5.0.2 Goal of the thesis

In this thesis we want to focus on which method the residuals actually resides in and try to focus on re-introducing parts of the sky eliminated in the U66 mask. Finding the methods which contains the residuals are important for many reasons, one of them being that one can improve all of the methods by finding out what works and does not work in the different methods.

5.1 Replicated work

As we can see from the plots of $\frac{x-\langle x\rangle}{\sigma_x}$ for both single method and difference map, we can see that we are basically spot on for the single method, and can proceed difference map. From the difference map plots we see that the overall form of the plots are the same, but due to the correction factor in the article (Axelsson et al. 2014[1]) that i have not included the values are not the same. This should not be that important, and i will come back to this in the discussion section.

5.2 Correlation coefficients

If we first look at the methods including CR combinations we see that they are spread more. We can also observe that it seem like CR method has the lower correlation coefficient in all of the combinations meaning that the foreground residuals comes from the other methods.

If we then look at the difference maps for the combinations without CR, we can clearly see that for they are packed closer together than the combinations with CR. Further we see that the combination of Nilc and Smica the correlation factors are more or less inseparable. This can either mean that there are hardly any residuals left in this combination, or that the residuals that are left in this combination are on the same order for both of the methods. Keeping this in mind we see that the combinations of these two methods with Sevem also have correlation efficients that are very small, with Sevem being the smaller one in both combinations. This means that the residuals in the foreground do not stem from the Sevem method.

5.3 Conclusion

If we only look at which of the methods that have the lower correlation coefficient in all of the combination we conclude with that the methods with least amount of residuals are CR, followed by SEVEM and finally SMICA and NILC with similar level of residuals. This is opposite result from what one would expect from all of the Planck publications. But as I have stated earlier we see that the combinations with CR are more spread out. In addition to that we have that the spread is so significant to the other combination that I have to conclude that there are a huge amount of residuals in these combination that they stem from both methods in the combinations with CR.

Now excluding the CR combinations, but still remembering that there are residuals in the remaining methods we can look at the more tightly packed correlation coefficients. We see that the values here are more or less the same for the combination with NILC-SMICA. This means that the residuals are on the same order for both of them and for the combination with Sevem the difference in coefficients are not big enough to conclude that Sevem is the better method.

So finally I think that for $j = 2$ meaning that we are looking at the largest scales in the universe, the CR method is clearly best. This is because the spread in correlation coefficients is not that great, but when we go to $j = 3$ or $j = 4$ the spread in the coefficients becomes to large to safely say something about the signal because of the foreground residuals. For the remaining methods the residuals are to big to say anything safely about the best method for foreground cleaning, but it looks like Sevem is the better method.

5.4 Sources of error

Following the code in Axelsson et al. 2014[1] we manage to replicate the results for single method analysis. But for difference maps, we have not included the correction factor. This should not be a big factor in the coefficients for a single combination, but for the comparison of combinations it might have a small effect.

The smoothing of the maps to a common resolution might also introduce a source of error for the correlation coefficient as the noise pictures gets warped for the different methods.

Further there is also a chance of systematic numerical errors for the operations that are done. This is of course something that should happen to each simulation and combination and can easily be checked by putting in a reference map where we know the outcome.

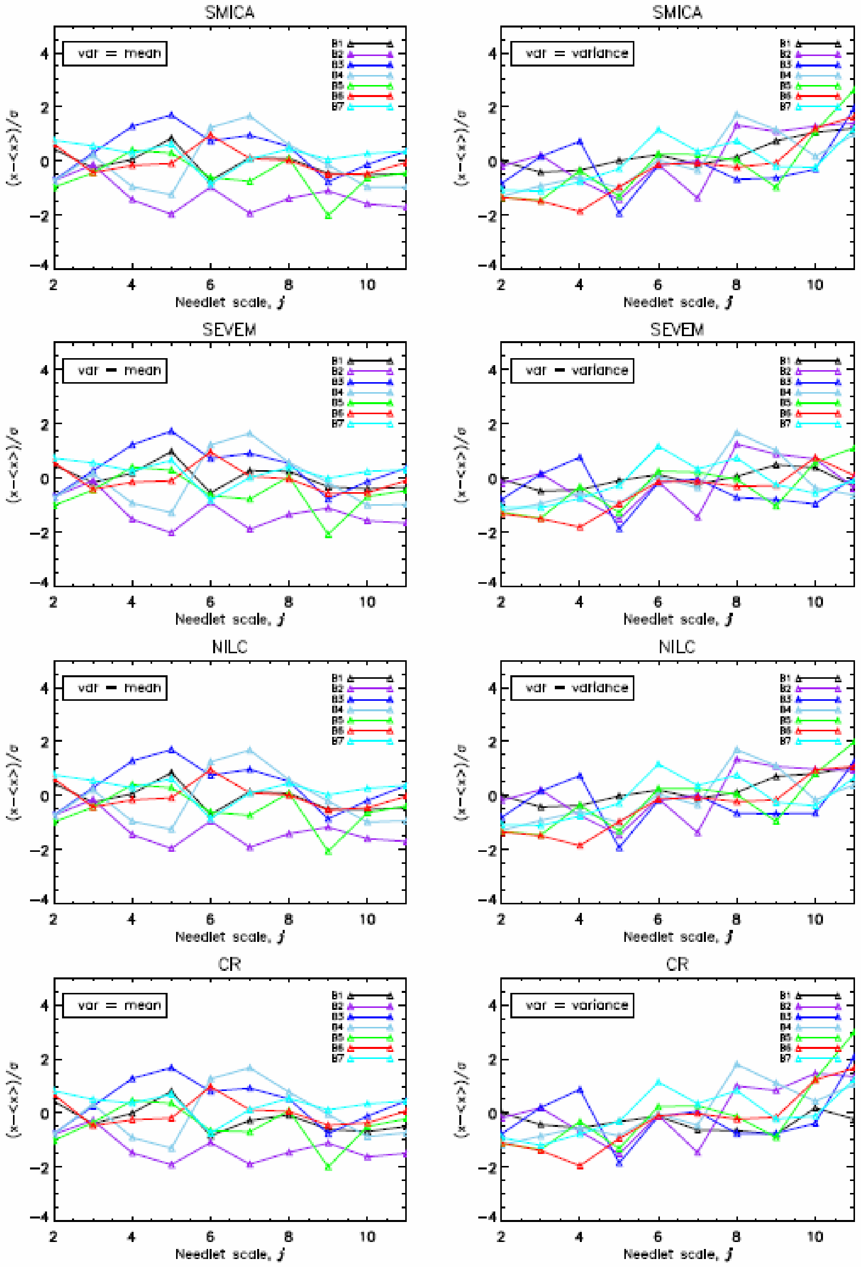

Figure 5.1: The results for single method from Axelsson et al. 2014[1]

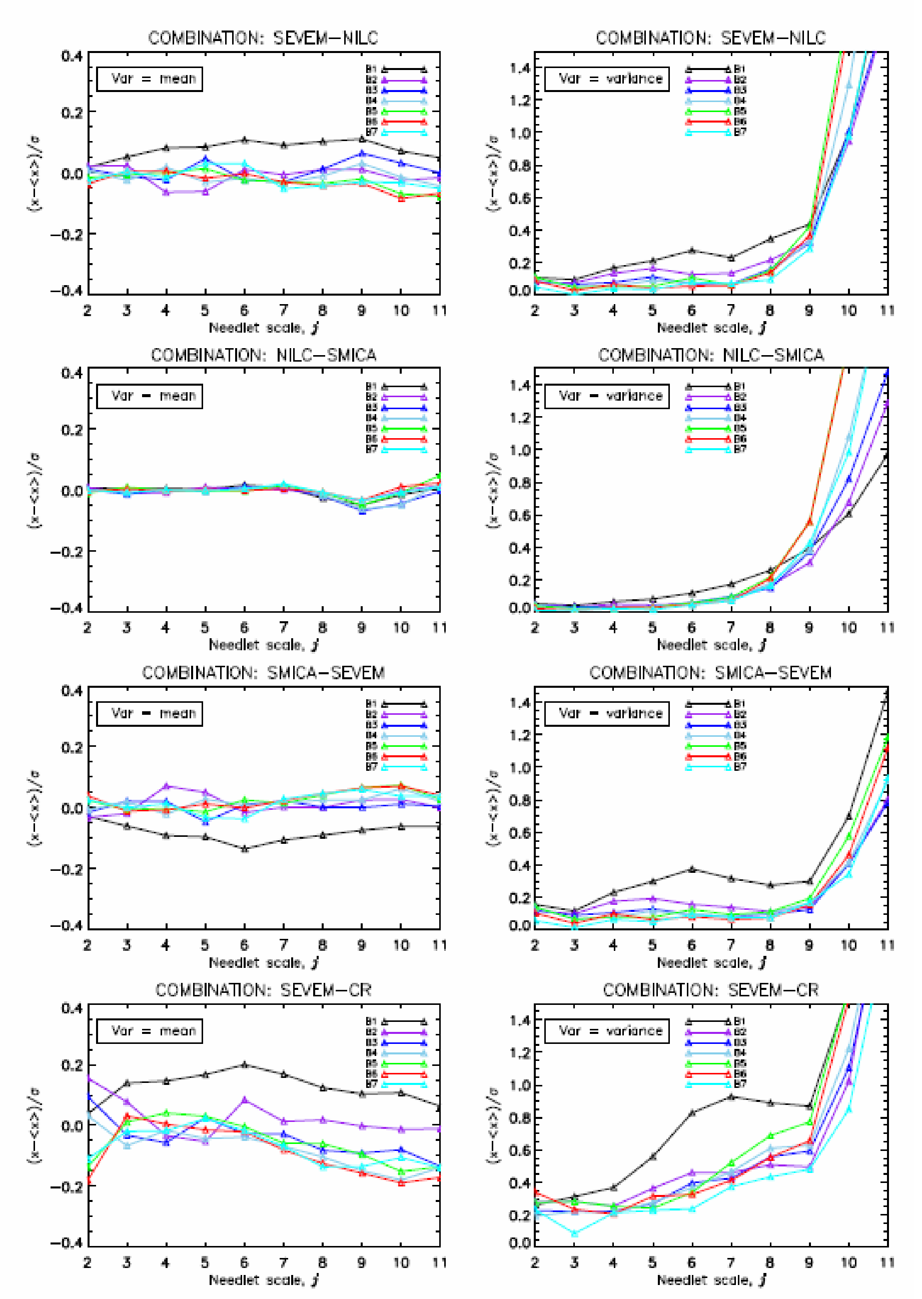

Figure 5.2: The results for difference map from Axelsson et al. 2014[1]. In the article they have chosen a subset of all the methods.

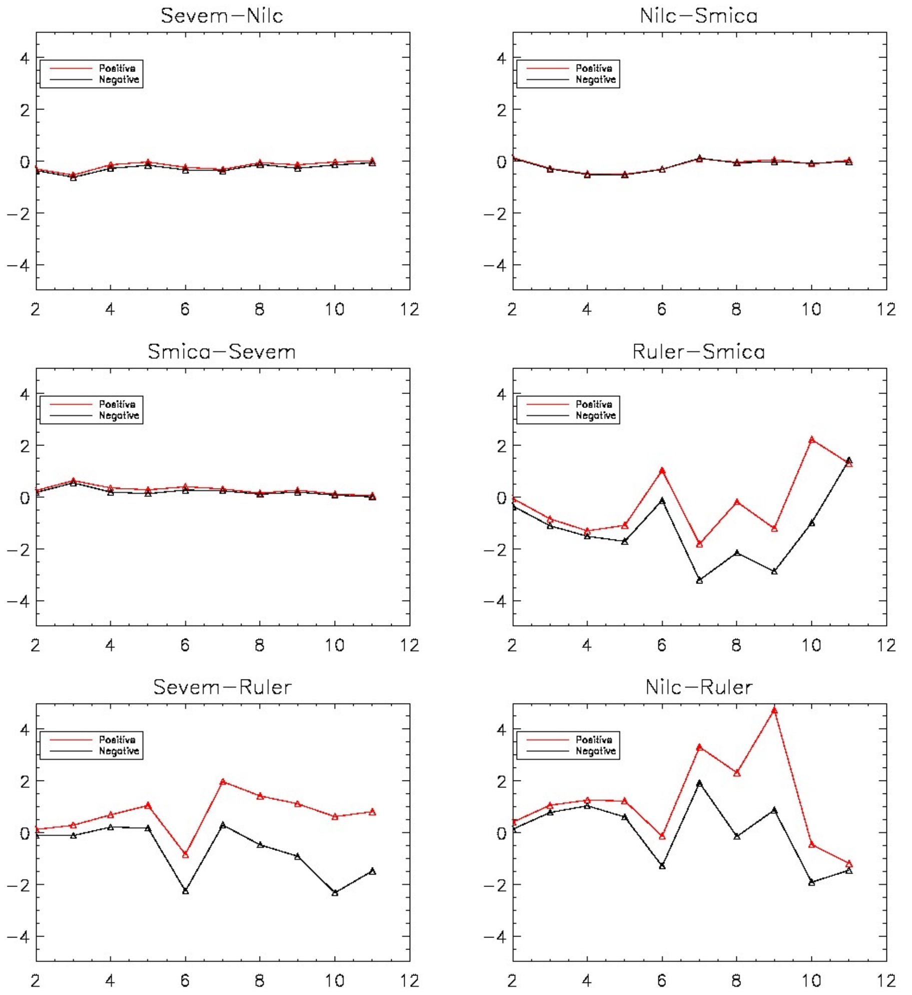

Figure 5.3: In this figure we can see the cross-correlation factor for the six different difference maps that is included in this thesis (shown on the form $\frac{x - \langle x \rangle}{\sigma_x}$). We can see that the combinations without Commander-Ruler method are more tightly together for all of the values of j.

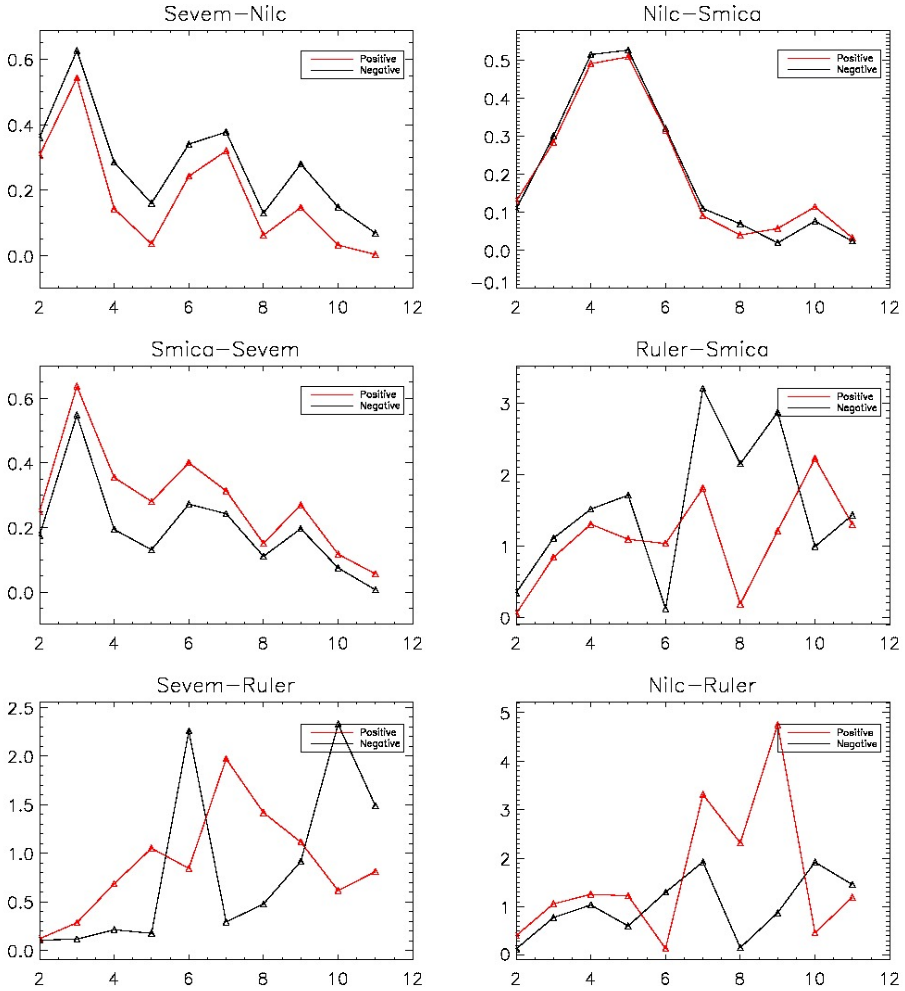

Figure 5.4: In these plots we have plotted the same as in figure 5.3. The only difference is that now we have taken the absolute value of the data to see which methods are closer to zero. The plots are also zoomed in so that it is easier to see differences in the plots.

Chapter 6

Further Work

In this thesis i have mostly focused on which of the methods that have the largest residuals near the galaxy. After this is done one can switch the focus over to where on the maps the residuals actually resides. This can be done quiet easily by switching how the correlation coefficients are computed. Instead of computing the coefficient for each simulation in band 1, one can compute the coefficient for each pixel by using the same pixel in the different simulations as a set of data.

By doing this one can try to go the other way as well, instead of trying to exclude more pixels from the U73 mask we can try to look at pixels that are excluded in the mask and show that they might be worth including as they do not introduce any foregrounds for the methods used.

There are also some minor discrepancies in the results obtained by myself in the replication of the work done by Axelsson et al. 2014[1] due to the bias factors created by looking at the jack-knife maps, that are not included in this thesis, and might influence the results slightly.

Building on the result of the work that can be done after this one might be able to see if there are something one can introduce to the foreground cleaning methods and ultimately better them as well.

List of Figures

1.1 Planck fluctuation map 2

2.1 Foreground examples 3
2.2 Foreground Frequency dependence 4
2.3 Weights for SMICA linear combination 6

3.1 Spherical harmonics example 10
3.2 Power Spectrum Example 11
3.3 Cosmological parameters in Power spectrum 12
3.4 Tweaking Dark matter content to see the effect on Power spectrum 13
3.5 Band Structure in U73 mask 15
3.6 Scale examples 16

4.1 Replicated mean and standard devation for singla analysis . . 22
4.2 Replicated mean for difference maps 23
4.3 Replicated standard deviation for difference maps 24

5.1 Results from Axelsson et al. 2014[1] single method analysis . . 28
5.2 Results from Axelsson et al. 2014[1] difference maps 29
5.3 Correlation coefficients 30
5.4 Correlation Coefficient zoomed 31

Bibliography

[1] M. Axelssons, H. T. Ihle, S. Scodeller, F.K. Hansen: *Testing for foreground residuals in the Planck foreground cleaned maps: A new method for designing confidence masks.* arXiv:1410.7102 [astro-ph.CO] October 28 , 2014.

[2] Planck Collaboration: *Planck 2013 results. XII. Component separation.* arXiv:1303.5072 [astro-ph.CO] March 22, 2013

[3] Kiyotomo Ichiki: *CMB foreground: A concise review.* Prog. Theor. Exp. Phys. (2014) 2014 (6): 06B109 doi:10.1093/ptep/ptu065 June 11, 2014

[4] D. Marinucci, D. Pietrobon, A. Balbi, P. Baldi, P. Cabella, G. Kerkyacharian, P. Natoli, D. Picard, N. Vittorio: *Spherical Needlets for CMB Data Analysis.* arXiv:0707.0844 [astro-ph] February 1, 2008

General References:

- `http://healpix.sourceforge.net/`
- Course in Cosmology II with H.K.K.Eriksen 2015 at UiO (University of Oslo)
- `http://www.cosmos.esa.int/web/planck`
- `https://en.wikipedia.org/wiki/Spherical_harmonics`
- `https://en.wikipedia.org/wiki/Correlation_and_dependence`
- `https://wiki.cosmos.esa.int/planckpla/index.php/CMB_and_astrophysical_component_maps`
- Sara Clausen Jønvik: *An Introduction to CMB analysis*; August,2016